Research Article | Vol. 30, No. 15 / 18 Jul 2022 / Optics Express 28190

Optics EXPRESS

Achieving sub-nanometer roughness on aspheric optical mold by non-contact polishing using damping-clothed tool

PENGFEI ZHANG,[1,2] LINGUANG LI,[1] ZHE YANG,[1] BO PAN,[1] MENG ZHANG,[1] XIAOGUANG GUO,[1] GANG LI,[2] DAEWOOK KIM,[3,4] AND JIANG GUO[1,*]

[1]*Key Laboratory for Precision and Non-traditional Machining Technology of Ministry of Education, Dalian University of Technology, Dalian 116024, China*
[2]*Key Laboratory of Chemical Lasers, Dalian Institute of Chemical Physics, Chinese Academy of Sciences, Dalian 116023, China*
[3]*James C. Wyant College of Optical Sciences, University of Arizona, 1630 E. University Blvd., Tucson, Arizona 85721, USA*
[4]*Department of Astronomy and Steward Observatory, University of Arizona, 933 N. Cherry Ave., Tucson, Arizona 85721, USA*
[*]*guojiang@dlut.edu.cn*

Abstract: The surface quality of optical lenses is highly required in imaging functions. Normally, ultra-precision turning is employed to fabricate the optical lenses. However, ultra-precision turning cannot meet the surface quality demands due to the tool marks. In this study, a new damping-clothed (DC) tool and chemical enhanced non-Newtonian ultrafine (CNNU) slurry for non-contact polishing are proposed to achieve sub-nanometer roughness on aspherical optical molds. A material removal model based on the hydrodynamic pressure and velocity simulation was established to calculate the dwell time in curved surface machining. The formation mechanism of sub-nanometer roughness is clarified. The proposed method and slurry were verified by the experiments in processing NiP alloy aspheric optical mold. After the process, surface roughness Sa achieved 0.54 nm and the form accuracy is less than PV 600 nm.

1. Introduction

Surface roughness is regarded as a critical evaluation parameter for the optics performance. Especially with the rapid development of consumer electronic products, the requirements for the precision and accuracy of optical components with imaging functions such as optical lenses are getting extremely high [1,2]. The surface roughness requirements of optical components such as aspheric surfaces and free-form surfaces have increased to the nanometer/sub-nanometer level or even the atomic level [3,4].

Over the past few decades, great progress has been made in the development of advanced polishing methods to meet the ultra-precision machining requirements of optical components [5] Such as bonnet polishing [6], magnetic field-assisted polishing [7], electrochemical polishing [8], and electron beam polishing [9] technology, etc. Among them, contact polishing methods such as bonnet polishing are easy to produce polishing marks due to the direct contact between the tool and the workpiece [10,11]. For optical components with imaging functions, the intermediate frequency error caused by the polishing marks will cause the light to scatter at a small angle during the transmission process, thereby reducing the resolution of the optical system. Other polishing techniques such as electron beam polishing and ion beam polishing have the problems of expensive equipment and low efficiency. In the field of optical finishing, polishing with fluids seems to work well [12]. For example, magnetorheological polishing technology is used for

#465975 https://doi.org/10.1364/OE.465975
Journal © 2022 Received 5 Jun 2022; revised 29 Jun 2022; accepted 30 Jun 2022; published 15 Jul 2022

Optics EXPRESS

polishing optical components due to its high flexibility and good surface quality, but it also has the problem of expensive equipment [13].

Non-Newtonian fluids make liquid bulletproof and water walking possible due to their shear thickening (ST) effect. In recent years, the ST effect has received great attention from researchers in the field of ultra-precision machining [14,15]. Selim et al. [16] mixed polyethylene glycol and nano-silica to obtain a non-Newtonian fluid base fluid. The steel bars were polished by adding SiC to the base fluid, and the surface roughness decreased from 0.46 μm to 0.24 μm. By optimizing parameters such as process angle and abrasive concentration, Nam [17] realized the polishing of complex features molds by non-Newtonian fluid, and the maximum surface pressure during the process could reach 7.95 kPa. Li et al. [14] used the slurry rotation method to finish the Cr12Mo1V1 material, and the roughness was reduced from Ra 105.95 nm to Ra 5.1 nm. Although the full aperture polishing method adopted by the above researchers can achieve good roughness, the control of form accuracy is uncertain. For optical components with imaging functions, form accuracy must be considered because it is related to the occurrence of systematic aberrations, astigmatism, etc. [18]. Zhu et al. [19,20] proposed a polishing method using sub-apertures, which greatly increases the certainty of the non-contact polishing process. However, high performance is often required for imaging components, which requires sub-nanometer or even atomic level roughness [21,22]. At present, non-contact polishing methods based on non-Newtonian fluids have not yet achieved sub-nanometer roughness on curved surfaces, which cannot meet the high-performance requirements of curved surface with imaging functions.

In this study, to meet the performance and precision requirements of optical components with imaging functions. A new non-contact polishing DC tool and CNNU slurry are proposed to obtain sub-nanometer roughness. The effect of working gap and tool speed on material removal rate (MRR) was studied by the proposed simulation and material removal model. Finally, the sub-nanometer roughness was realized on the NiP alloy curved surface by the proposed DC tool and CNNU slurry, and its formation and evolution law were clarified.

2. Methodology

2.1. Principle

The DC tool is proposed in this study based on the ST effect of CNNU fluids. The substrate of the DC tool is made of aluminum alloy with a diameter of 12 mm. A semi-rigid damping layer is adhered to the surface of the aluminum alloy substrate. The DC tool is small in dimension and can be well adapted to the form of small aperture optical components. Due to the existence of the damping layer, the DC tool can stably drive the CNNU slurry to rapidly reach the peak of the thickening curve and fluctuate in the highest viscosity region. As shown in Fig. 1, during the non-contact polishing process, the working gap between the DC tool and the workpiece and the tool speed is kept constant. The process angle is set to 60°. The curved workpiece surface is subjected to the combination of hydrodynamic pressure and ST, material is removed without contact. In the non-contact polishing process, the influence and removal zone are formed on the flat/curved surface by the combination of ST and hydrodynamic effects.

CNNU slurries were prepared to meet non-contact polishing process requirements. The CNNU slurry was prepared by mixing colloidal silica, polyhydroxy polymer, hydrogen peroxide concentration and deionized water. Figure 2 shows the interaction between the workpiece and the DC tool in the gap during the non-contact process using CNNU slurry. The CNNU slurry was ejected by the nozzle and flowed into the removal interface and was induced by the DC tool to form a hydrodynamic pressure affected zone in the wedge gap. Surface material in the pressure-affected zone is removed by particle clusters formed by ST. The oxidized material is continuously removed under the chemical action of hydrogen peroxide in the CNNU slurry.

Optics EXPRESS

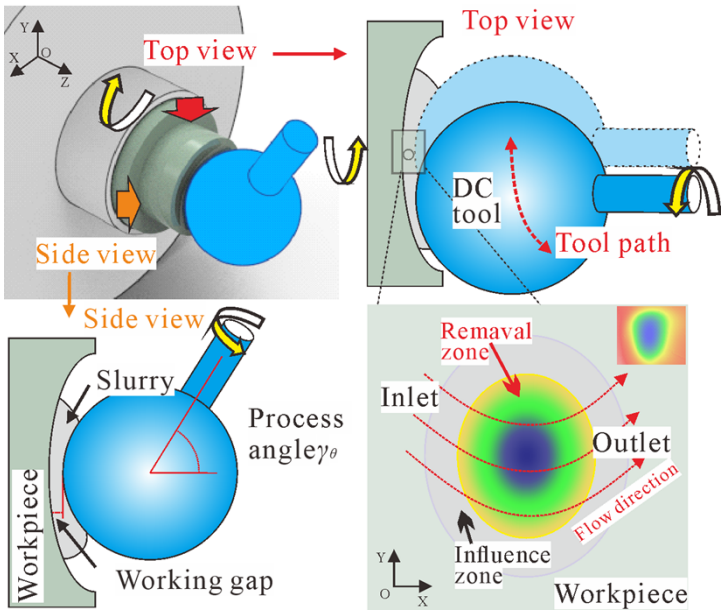

Fig. 1. Schematic diagram of the non-contact polishing process using DC tool.

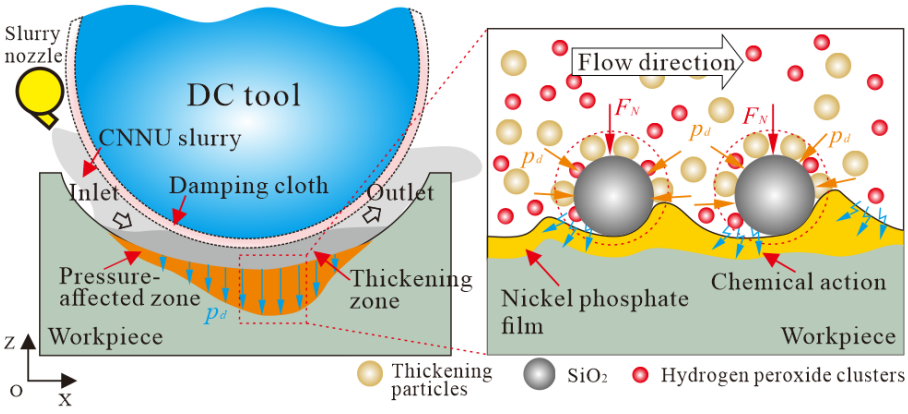

Fig. 2. Schematic diagram of the mechanism of CNNU slurry in the non-contact polishing process with DC tool.

Optics EXPRESS

2.2. Finite Element Model (FEM)

The pressure and velocity distributions in the wedge gap were analyzed by the finite element method. The flow of CNNU fluid in the polishing process, the schematic diagram of velocity gradient u and the shear force τ of the workpiece at the wedge gap are shown in Fig. 3(a). The boundary conditions of the model are shown in Fig. 3(b). The inlet boundary condition is set as 'Velocity inlet', the direction is perpendicular to the boundary, and the value corresponds to the linear velocity v_{tt} of tool speed. The outlet boundary condition is set as 'Zero pressure'. The tool and workpiece boundaries are set as no-slip boundaries I and II, respectively. The constitutive relation is defined as inelastic non-Newtonian, and the inelastic model is set as power law. The tool radius is set to 6.25 mm. The consistency constant K is set to 0.62. the flow behavior index n was set to 1.5, The fluid density ρ was set to 1.43 g/ml according to the experimental test. Based on the rheological test results, the reference shear rate was set to 120 s^{-1}. The tool speed and working gap were set to 5000 rpm and 0.1 mm, respectively.

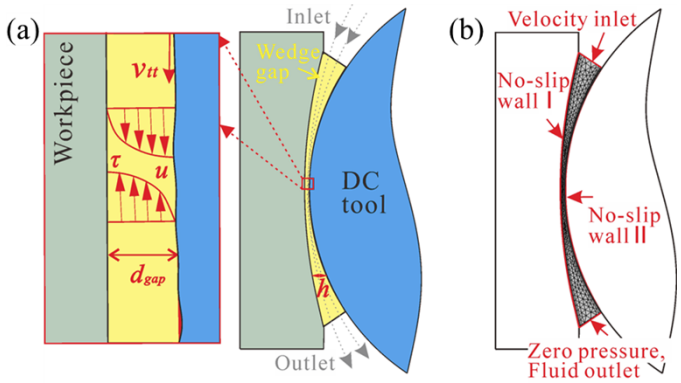

Fig. 3. (a) Model setup and simulation (b) boundary conditions during the DC tool non-contact polishing.

2.3. MRR in non-contact polishing using DC tool

To clarify the material removal process during DC tool non-contact polishing process, it is important to establish the MRR mathematical model. The material removal mechanism during non-contact polishing by DC tool is explored in this section. Material removal is mainly attributed to the mechanical removal of the NiP alloy surface material by the SiO_2 abrasive particles in the CNNU slurry. The material removal model according to Ref. [23] can be written as:

$$MRR_{\mathrm{t}} = k_0 \int_t V_t dt \tag{1}$$

where V_t is the total removal volume, and k_0 is the modified coefficient.

Based on the Hertzian contact theory, the penetration depth of a single SiO_2 abrasive in the wedge gap depends on the positive pressure F_N of the abrasive. According to related research, F_N can be expressed as [24]:

$$F_N = \frac{\sqrt{3} p_{\mathrm{d}} \cdot D_{\mathrm{a}}^2}{2 f_{\mathrm{t}}} \tag{2}$$

where f_t is the contact networking coefficient of SiO_2. D_a is the diameter of SiO_2, p_d is the hydrodynamic pressure obtained from the FEM.

Optics EXPRESS

During the DC tool non-contact polishing process, the CNNU slurry forms a semi-solid steady fluid in the wedge gap, and the SiO_2 abrasive micro-cutting of the semi-solid particle cluster on the workpiece results in material removal. The mathematical model of the relationship between abrasive grains and materials is shown in Fig. 4.

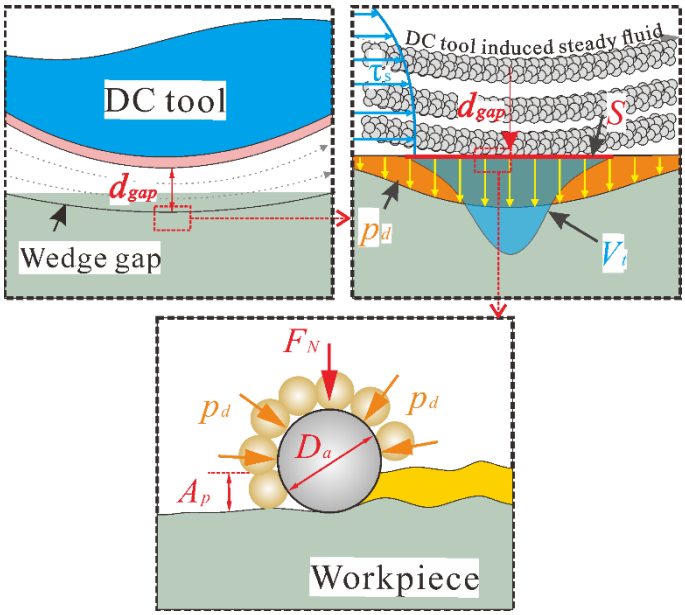

Fig. 4. Schematic sketch of material removal during non-contact polishing using DC tool.

Total removal volume V_t can be expressed as:

$$V_t = N_a V_{sa} \tag{3}$$

where N_a is the total number of active abrasives, V_{sa} is the removal volume of a single abrasive.

The indentation depth of a single SiO_2 abrasive can be calculated as [25]:

$$A_p = \frac{F_N/g}{\pi D_a H_W} \tag{4}$$

where g is constant and is usually taken as 9.8 m/s, H_W is the Vickers hardness of the NiP alloy substrate.

During the non-contact polishing by DC tool, the removal volume of a single abrasive V_{sa} can be written as [26]:

$$V_{sa} = k_0 \pi D_a A_p^2 dt \tag{5}$$

According to Eqs. (2) and (4) A_p can be expressed as:

$$A_p = \frac{\sqrt{3} p_d D_a}{2\pi g f_t H_W} \tag{6}$$

Similarly, removal volume of a single abrasive V_{sa} can be written as:

$$V_{sa} = k \frac{3 p_d^2 D_a^3 dt}{4 g^2 f_t^2 H_w^2} \tag{7}$$

Optics EXPRESS

The total number of active abrasives N_a in the removed area within the wedge gap can be written as [27]:

$$N_{\mathrm{a}} = Sv_{tt}\rho_{\mathrm{p}} \tag{8}$$

where cross-sectional area S of the CNNU slurry flowing through the workpiece surface can be obtained from the experimental results (16π mm^2), ρ_p is the volume density of SiO_2 abrasives contained in the CNNU slurry. The effective relative velocity v_{tt} is related to the process angle of the DC tool, v_{tt} can be expressed as:

$$v_{tt} = v_t sin\gamma_\theta \tag{9}$$

where v_t is the maximum linear velocity of the DC tool, $v_t = 2\pi \mathrm{R}n$, R is the tool radius, n is the tool speed, γ_θ is the process angle.

According to related research [27], the volume density ρ_p of the abrasive grains number contained in the polishing liquid can be written as:

$$\rho_p = \frac{3d_{\mathrm{s}}\rho_{\mathrm{s}}m_a}{4\pi {D_a}^3\rho_{\mathrm{a}}} \tag{10}$$

where d_s is the dilution rate of the slurry, ρ_s is the density of CNNU slurry, m_a is the mass fraction of SiO_2 abrasives in the CNNU system, ρ_a is the density of SiO_2.

Substituting Eqs. (8), (9) into Eq. (7), the total number of active abrasives N_a can be expressed as:

$$N_{\mathrm{a}} = \frac{3Snd_{\mathrm{s}}sin\gamma_\theta\rho_{\mathrm{p}}\rho_{\mathrm{s}}m_a}{4D_a^2\rho_{\mathrm{a}}} \tag{11}$$

Therefore, the total removal volume V_t can be expressed as:

$$V_t = Su\rho_{\mathrm{p}} \cdot k\pi D_x \mathrm{A}_{\mathrm{p}}^2 dt = \frac{9kSp_d^2D_ad_ssin\gamma_\theta\rho_{\mathrm{s}}m_a}{16g^2f_t^2H_w^2\rho_{\mathrm{a}}}dt \tag{12}$$

Consequently, the theoretical removal rate MRR_t can be written as:

$$MRR_{\mathrm{t}} = \frac{9kS}{16g^2}\int_t \frac{p_d^2D_ad_ssin\gamma_\theta\rho_{\mathrm{s}}m_a}{f_t^2H_w^2\rho_{\mathrm{a}}}dt \tag{13}$$

The influencing factors of material removal can be conveniently obtained from Eq. (13) for the purpose of polishing process control. In the non-contact polishing process by DC tool, the MRR is mainly related to hydrodynamic pressure p_d, the diameter of SiO_2 D_a, process angle γ_θ, the density of CNNU slurry ρ_a, and mass fraction of SiO_2 abrasives ρ_a. The hydrodynamic pressure p_d is greatly affected by the tool speed n and working gap d_{gap}.

3. Experimental

In this work, a high-precision CNC machine with 2 spindles and 2 moving axes was used to carry out the experiment. As shown in Fig. 5, the flat and curved NiP alloy workpieces are mounted on the spindle I through a fixture, and the spindle II is connected to the Z axis through an XYZ micro-displacement platform. The CNNU slurry is transported to the removal interface through the supply pipeline. The tool and workpiece were adjusted to the specified distance by moving the Z axis. The rotational speed of spindle II with DC tool installed can be adjusted between 100 and 12000 rpm. The rotational speed of the spindle I can be adjusted between 0-3000 rpm. The positioning accuracy of the XZ axis is ±2 μm. As shown in Table 1, the working gap interval used during the experiments was 0.01–0.3 mm, the tool speed was 2000, 5000 and 8000 rpm, and the workpiece rotational speed was 100 rpm.

Optics EXPRESS

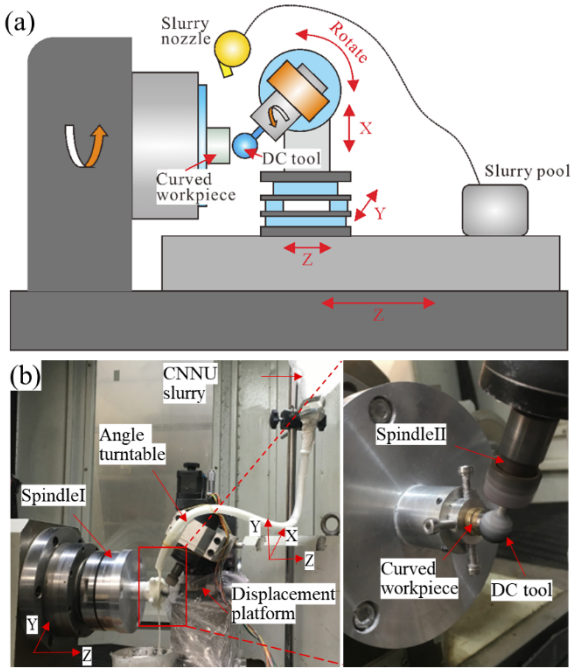

Fig. 5. Experimental setup (a) Schematic diagram and (b) device for curved surface by using DC tool.

The properties of CNNU slurries have a crucial impact on the experimental performance. The high-performance slurries composition and ratio were obtained through previous empirical experimental studies. The proportion of polyhydroxy polymer is 58 wt% in the base fluid, and the concentration of SiO_2 abrasive particles in the system was 10 wt%. The hydrogen peroxide concentration is 1 wt%. The specific parameters of the CNNU slurry are shown in Table 2.

Table 1. Experimental parameters

Parameter category		Numerical value
Tool speed	n	2000, 5000, 8000 rpm
Working gap	d_{gap}	0.01, 0.1, 0.2, 0.3 mm
Diameter of SiO_2	D_a	20 nm
Vickers hardness of the NiP alloy	H_w	0.53×10^3 kg/mm^2
Process angle	γ_θ	60°
Density of CNNU slurry	ρ_s	1.43 g/ml
Mass fraction of SiO_2 abrasives	m_a	10%
The density of SiO_2	ρ_a	2.2 g/cm^3
Cross-sectional area	S	16π mm^2
Time per circle	t	30 min

Before and after polishing experiments, the workpieces were ultrasonically cleaned in deionized water and alcohol. The rheometer (MCR302, Anton Paar, Austria) was used to analysis the rheological properties of the configured CNNU fluids. The surface morphology of NiP alloy was observed using a super depth of field microscope (VHX-600E03041132, KEYENCE, Japan) and a

Optics EXPRESS

Table 2. CNNU Slurry Composition

Composition	Proportion
Base fluid	89 wt% (Polyhydroxy polymer accounts for 58 wt% of the base fluid)
SiO_2 concentration	10 wt%
Hydrogen peroxide concentration	1 wt%

scanning electron microscopy (Q45, FEI, USA) before and after polishing. The three-dimensional topography and roughness of the workpiece surface were measured by a white light interferometer (NewView9000, Zygo, USA). The objective lens used for measurement is 10× (Zygo), the measurement and analysis range both are 200×200 μm. The roughness was evaluated using the arithmetic mean deviation (Sa), using a Gaussian high-pass filter with a cut-off length of 80 μm. The crystal structure of the NiP alloy was characterized via X-ray diffractometry (EMPYREAN, PANalytical, Netherlands) before and after the experiment. The surface profile of the workpiece was measured using a Taylor contact profilometer (Form TalySurf PGI 840, Taylor Hobson, UK).

4. Results and discussion

4.1. Rheological properties

The rheological properties of CNNU slurry are related to the roughness obtained and the material removal ability [28,29]. The rheometer was used to test the rheological properties of the prepared CNNU slurries. The lamina with a diameter of 34.14 mm was selected to conduct the test, the included angle of the lamina surface was 5°, the test gap was set to 0.101 mm, and the shear rate variation range was set to 0.1-1500 s^{-1}. The results are shown in Fig. 6 The prepared SNNU slurry conforms to the rheological characteristics of non-Newtonian fluids and has an obvious ST effect. CNNU dispersion system showed three obvious viscosity variation ranges: Zone I, Zone II, and Zone III. Zones I and III are shear thinning zones, where the polyhydroxy polymer and abrasive particles in the CNNU slurry are in a free or excessive shearing state. The viscosity of the CNNU slurry in zone II increased continuously with the increase of the shear rate and showed the maximum viscosity when the shear rate was 130 s^{-1}, and the particles in the CNNU continued to aggregate. The critical shear rate of the CNNU dispersion system is 130 s^{-1}, and the maximum viscosity reaches about 25 Pa·s. The rheological properties of CNNU are comparable to those of Li et al [30]. Therefore, the prepared CNNU system has a strong thickening effect and can achieve continuous and stable material removal.

4.2. CNNU slurry performance analysis

Non-Newtonian ultrafine (NNU) and CNNU slurries were prepared to explore the effect of hydrogen peroxide in the polishing process. The composition of NNU is basically the same as CNNU, but do not contain hydrogen peroxide. Figure 7 shows the surface roughness and morphology of the initial, polished with NNU or CNNU slurry, respectively. Figure 7(a) shows the initial surface obtained by the contact polishing method. The initial roughness is Sa 2.95 nm with crossed scratches. The surface roughness was significantly reduced after being treated with NNU slurry, but the incompletely removed cross scratches could still be observed. As shown in Fig. 7(c), the surface roughness rapidly decreased to 0.90 nm and no defects were observed after being polished with CNNU slurry. The roughness obtained by the prepared CNNU slurry is better than that of the alumina and ceria systems [19,31]. Figure 7 shows that the CNNU slurry has strong surface smoothing ability to obtain defect-free surfaces, which is attributed

Optics EXPRESS

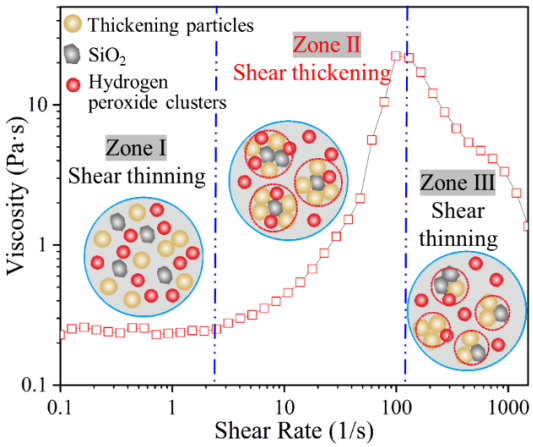

Fig. 6. Rheological curve of CNNU slurry system.

to the synergistic effect of mechanical shear and chemistry during non-contact polishing. NiP alloy surface material is removed by the DC tool induced shearing action of abrasive grains. In addition, new reactive layer are continuously generated on the surface material and are removed by the oxidation of hydrogen peroxide [32].

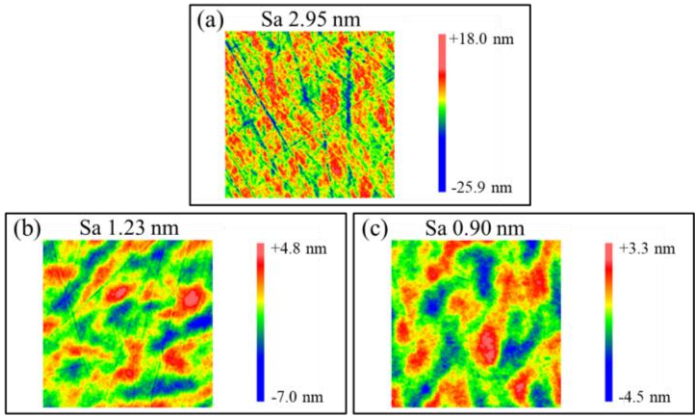

Fig. 7. Surface roughness and morphology of (a) initial, treated with (b) NNU and (c) CNNU slurry by DC tool.

Determining the material composition of the polished surfaces helps to further explore the material removal mechanism. X-ray diffractometer (XRD) was used to analyze the composition of the processed surface. Figure 8 shows the XRD collection results of the NiP alloy surface polished by NNU and CNNU slurries. The 2Theta range was set to 20-80° during the collection process. The test voltage and current were set to 40 kV and 40 mA, respectively. No obvious diffraction peak was observed on the surface polished with NNU, only the characteristic diffraction peak of NiP alloy at 45° was observed. Several strong diffraction peaks were found on the surface treated with CNNU. The film newly formed on the CNNU treated surface is monoclinic (MCL) $Ni_2P_4O_{12}$ and may be amorphous NiP_4O_{11}, which are found by comparing with standard PDF cards. The results showed that a new nickel phosphate film was generated on CNNU treated surface, and nickel phosphate was easily soluble in inorganic acid, which accelerated the material

Optics EXPRESS

removal efficiency. Due to the synergistic effect of chemical effects, ultra-smooth scratch-free surfaces can be obtained.

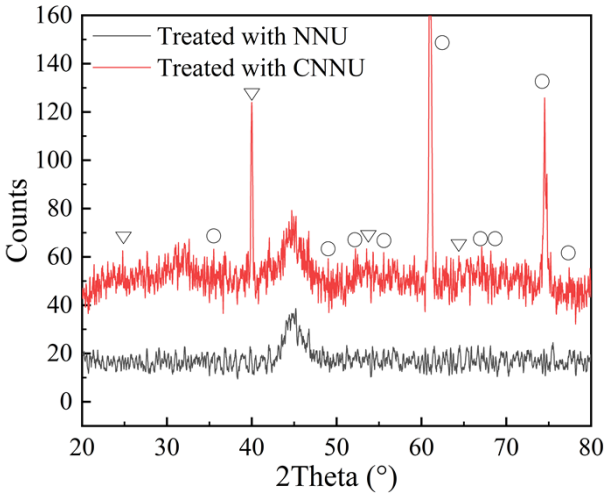

Fig. 8. XRD analysis of NiP alloy surface after polishing with NNU and CNNU slurries ($\circ Ni_2P_4O_{12}\nabla NiP_4O_{11}$).

4.3. *Hydrodynamic pressure p_h at different working gaps and tool speeds in the FEM*

Figure 9 shows the pressure and velocity distribution of the fluid in the wedge gap with a fixed working gap of 0.01 mm and a tool speed of 5000 rpm. The pressure can reach maximum of about 1640 kPa, and the pressure value at d_{gap} is about 700 kPa, which are shown in Fig. 9(a). The hydrodynamic pressure between the inlet and the d_{gap} is high, and the pressure gradually decreases as the fluid flows. The fluid pressure p_h is low and gradually decreasing from the d_{gap} to the outlet. The velocity distribution of the fluid is shown in Fig. 9(b). The simulation results show that the fluid velocity decreases gradually with the increasing gap.

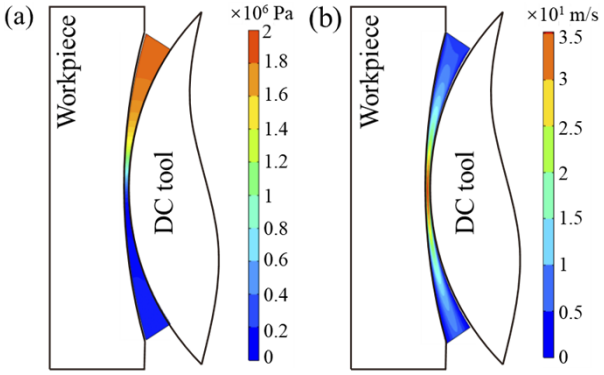

Fig. 9. (a) Pressure and (b) velocity distribution field nephogram.

Figure 10 shows the hydrodynamic pressure p_d obtained at d_{gap} based on the FEM. Figure 10(b) shows that p_d increases continuously with the increase of tool speed, and the change of p_d caused by tool speed is weaker than that of working gap. Interestingly, the p_d at d_{gap} decreases when tool speed exceeds 5000 rpm, which may be due to shear thinning that occurs when the shear rate

Optics EXPRESS

exceeds the critical shear rate. According to the relevant research [33], the yield stress of NiP alloy material is about 200 kPa. Effective material removal may not be obtained when working gap exceeds 0.2 mm.

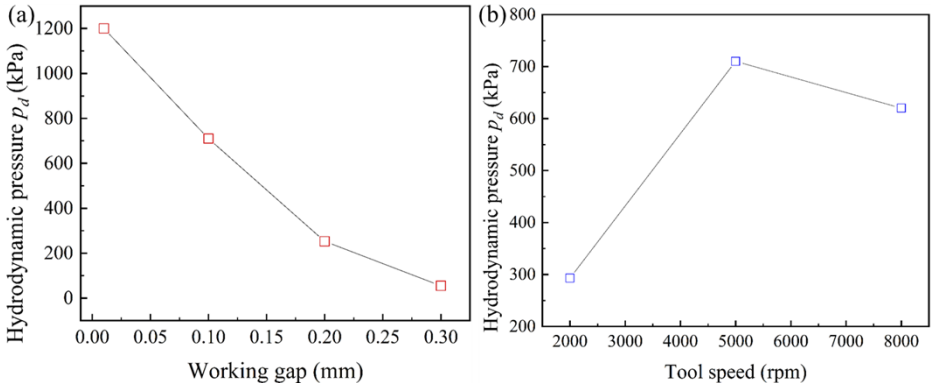

Fig. 10. Simulated p_d at different working gaps and tool speeds.

4.4. Prediction of MRR

Figure 11 shows the MRR_t under different working gaps and tool speeds predicted by the model. The coefficient k in Eq. (13) is corrected to $2.3e^{-9}$ using experimental data. Figure 11(a) shows that the MRR_t decreases with the increase of the working gap. The maximum MRR_t occurs at 0.01 mm. The predicted MRR_t at different tool speeds are shown in Fig. 11(b), and MRR_t increases with the increasing tool speed. The increase rate of MRR_t slowed down when the tool speed continued to increase and exceeded 5000 rpm. The maximum MRR_t occurs at 5000 rpm. The trend of the results is consistent with related research [19], and the predicted results provide a firm reference for the experimental parameters selection.

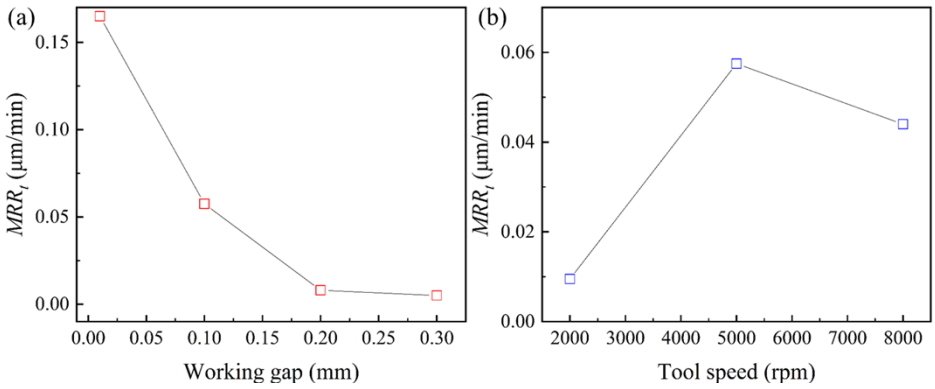

Fig. 11. Predicted MRR_t under different (a) working gaps and (b) tool speeds.

4.5. Experimental analysis of MRR

The predicted results in Fig. 12 show that working gap greatly influences both MRR_e and surface quality, as it affects the thickening effect of the polishing slurry and then affects the processing efficiency [24]. During the test, the tool speed was fixed at 8000 rpm, and the dwell time t was 30

Optics EXPRESS

min. The thickening degree of particle clusters has an impact on surface quality. Figure 12(a) shows that the MRR_e decreases continuously with the increasing working gap, which is basically consistent with the results of the predicted result MRR_t. The minimum MRR_e is 0.021 μm/min at 2000 rpm. At 5000 and 8000 rpm, the MRR_e is about 0.060 μm/min. Figure 12(b) shows that smooth profiles were obtained at working gap 0.1, 0.2 and 0.3 mm. Scratches appeared at the bottom of the removal profile at working gap 0.01 mm due to excessive particles aggregation [34].

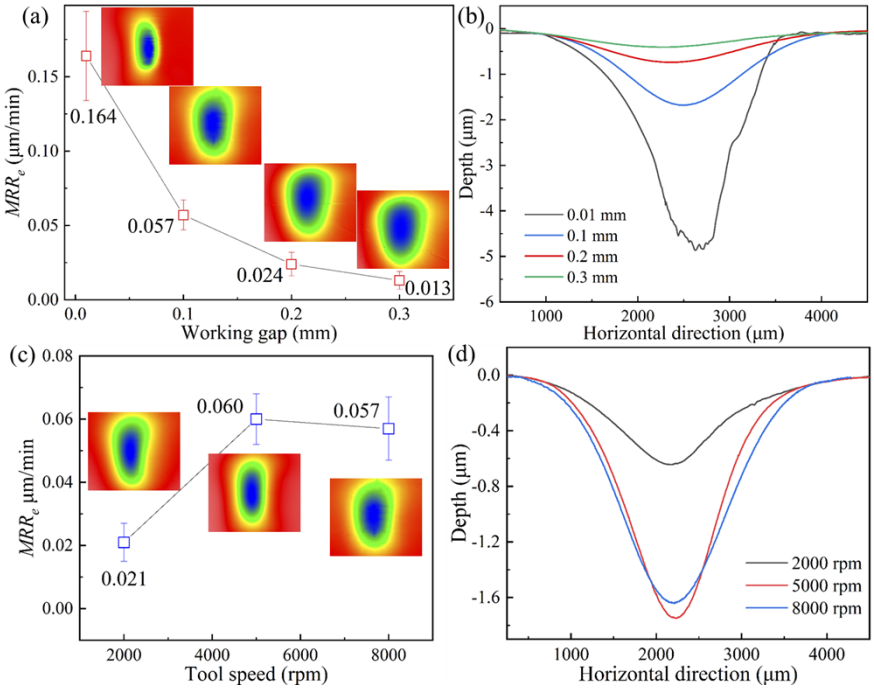

Fig. 12. Experimental (a) (c) MRR_e and (b) (d) cross-sectional profile at different working gaps and tool speeds.

The tool speed also plays a critical role in the obtained MRR_e, since the tool speed determines the shear rate of the polishing fluid and thus affects the MRR of the slurry [19]. Figure 12(c)(d) shows the material removal results obtained at different tool speeds with a fixed working gap 0.1 mm. The rotational speed used for the experiment were 2000, 5000 and 8000 rpm. Figure 12(c) shows that MRR_e increases with the increasing tool speed. The maximum MRR_e is 0.06 μm/min at 5000 rpm, and the minimum MRR_e is 0.021 μm/min at 2000 rpm, which is basically consistent with the results of the predicted trend. When the tool speed was increased from 5000 to 8000 rpm, the MRR_e remained basically unchanged or decreased slightly, which may be caused by the shear thinning of the CNNU slurry [34]. Figure 12(d) shows that continuous smooth removal profile can be obtained at 2000-8000 rpm.

4.6. Method performance comparison

The surface defect is an important part of optical performance evaluation. For optical components with imaging functions, the existence of pits, polishing texture and scratches will seriously affect the imaging quality [35]. To evaluate the smoothing ability of different processes on NiP alloy surface, the surface morphology and roughness produced by contact polishing, cutting, fabric-clothed (FC) and DC tool non-contact polishing were measured and analyzed. Uniform polishing is adopted in the process, the tool feed rate is 100 mm/min for both contact and

Optics EXPRESS

non-contact processes, and the contact polishing pressure is 1 N. Figure 13 shows the surface image and three-dimensional (3D) morphology produced by contact polishing, cutting, FC and DC non-contact polishing processes. As shown in Fig. 13(a), the contact polishing method produces crossed scratches. The surface obtained by cutting process in Fig. 13(b) produced continuous tool marks. The surface treated with the FC tool in Fig. 13(c) produced continuous scratches, and this surface deterioration may be due to the disordered aggregation of particles [19]. No scratches are observed on the surface using the DC tool in Fig. 13(d). Figure 13 also shows the surface roughness produced by contact polishing, cutting, FC and DC non-contact polishing. As shown in Fig. 13(a), the surface roughness after contact polishing is 3.03 nm with irregular tool marks. The surface roughness obtained by cutting in Fig. 13(b) is 3.15 nm, and obvious tool marks are observed on the surface. Figure 13(c) and (d) are the 3D topography of the surfaces obtained by the FC and DC tool non-contact polishing, and the roughness is 1.95 and 0.76 nm, respectively. The 3D topography measurements show that the best surface roughness is obtained by the DC tool non-contact polishing method. Figure 13(e)(f) shows the scanning electron microscopy (SEM) surface morphologies obtained by contact polishing and DC tool non-contact polishing. Figure 13(e) shows that the surface obtained by contact polishing has obvious scratches and pits, while no surface defects are observed by DC tools non-contact polishing. The above results show that the surface obtained by the DC tool is superior to that of the contact polishing, cutting and FC tools, and a smooth and defect-free surface can be obtained. Power spectral density function (PSD) is another way to characterize optical surfaces, which can provide more comprehensive information about the surface profile obtained. Figure 13(g) shows the PSD curves of the surfaces treated by different finishing processes. The results show that the value of mid and high-spatial frequency can be effectively suppressed by using non-contact polishing with DC tool, which helps to improve the performance of optical components.

4.7. Continuous removal capability of the DC tool

To investigate the removal ability of the DC tool, an experiment with a gradual working gap was carried out. As shown in Fig. 14(a), the horizontal length of the working trajectory is 5 mm, the working gap increases from 0.01 mm to 0.3 mm, and the feed rate is 0.01 mm/min. The obtained 3D profile of the removal shape is shown in Fig. 14(a), where it can be observed that the removal depth decreases with the increasing working gap. Figure 14(b) shows the profile of the A-A and B-B sections in Fig. 14(a), indicating that the DC tool non-contact polishing process used in this study has good continuous removal capability.

4.8. Performance analysis of curved surface

The experimental results of flat parts show that good roughness of Sa 0.76 nm can be obtained by DC tool non-contact polishing method. On this basis, an experimental study of optical aspheric mold polishing was carried out. The parameters used in this experiment are obtained from the above basic experiments, namely working gap 0.1 mm and tool speed 5000 rpm, and the workpiece speed is 100 rpm. During the test, take points at equal intervals (0.5 mm) along the radial direction of the workpiece and keep working gap 0.1 mm constant. Figure 15(a) shows the surface roughness variation and form profile of the NiP alloy surface treated with DC tool. Figure 15(a) shows that the roughness decreases continuously as the polishing process progresses and finally saturates to 0.52 nm. The initial surface roughness was 3.24 nm, which was obtained by the contact polishing method. As shown in Fig. 15(a)(b)(c), after being treated with the DC tool non-contact polishing, the crossed scratches were obviously removed, and the roughness was reduced to 1.30 nm. The surface roughness was saturated to 0.54 nm after continuous polishing for 4 h. The surface form accuracy is related to the imaging effect and performance of curved optical components, so it is vitally important to study the form change of curved surfaces during ultra-precision polishing [36]. The form data of the curved workpiece before and after

Optics EXPRESS

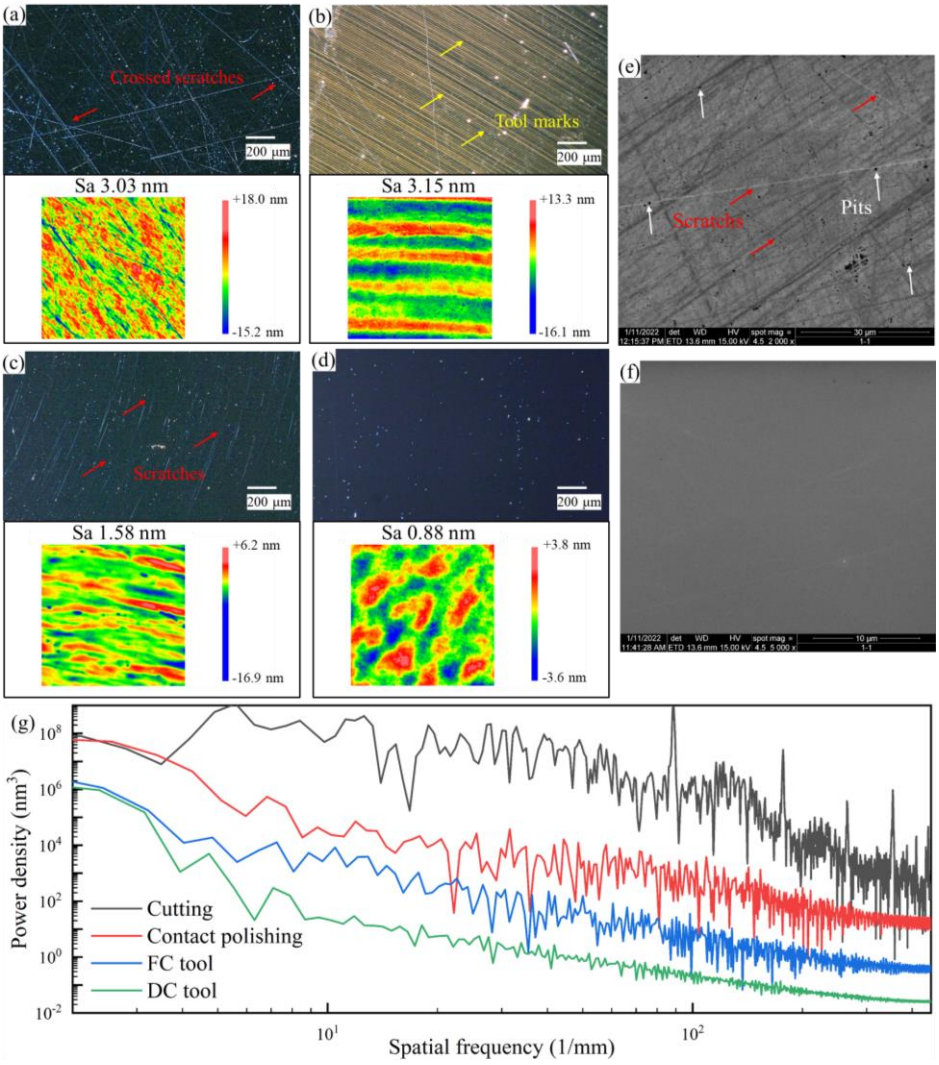

Fig. 13. Surface defects and roughness under (a) contact polishing (b) cutting (c) FC tool and (d) DC tool non-contact polishing, the SEM topography under (e) contact polishing and (f) DC tool non-contact polishing, and (g) PSD curve.

Optics EXPRESS

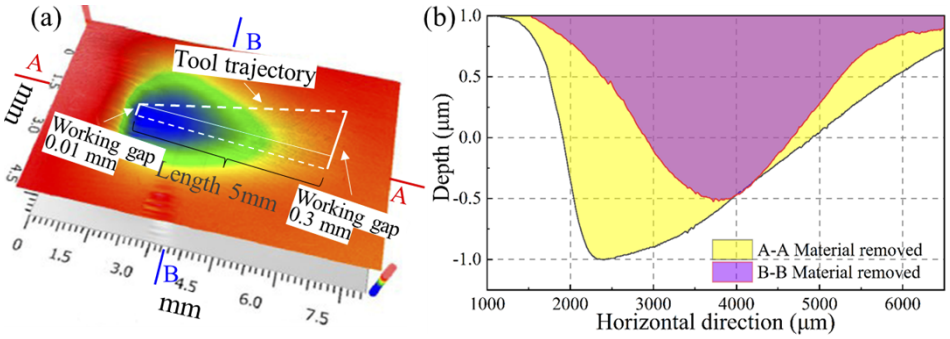

Fig. 14. (a) Tool trajectory and 3D morphology and (b) cross-sectional profile with continuous gradient working gap using DC tool.

polishing were measured by a Taylor 3D morphology instrument. MATLAB software was used to iteratively calculate the form error of the profile before and after polishing. Figure 15(d) shows that the form error due to DC tool non-contact polishing is less than 600 nm.

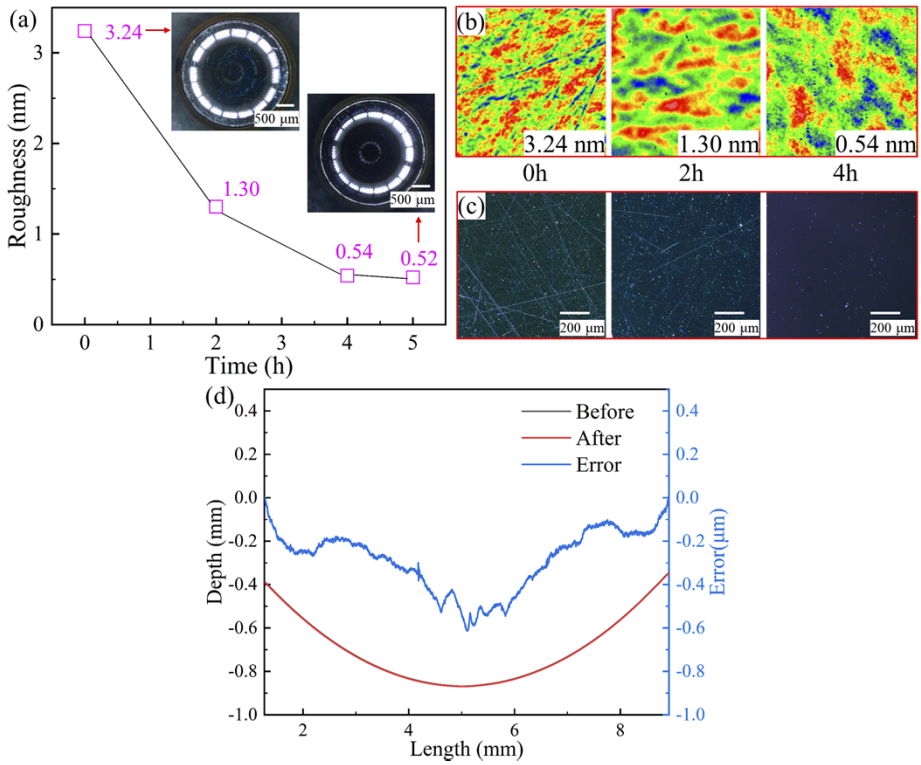

Fig. 15. (a) Roughness variation, (b) surface roughness, (c) defects of curved optics and (d) form error at different stages of aspheric optical surface processed using DC tool.

5. Conclusions

In this paper, a new DC tool and CNNU slurry for non-contact polishing were proposed for aspheric optical mold fabrication, and a material removal model based on hydrodynamic pressure

Optics EXPRESS

and velocity simulation was established. Besides, the influence of working gap and tool speed on material removal of the DC tool was studied through theoretical analysis and experiments, and the optimal parameters were obtained for curved surface polishing. The main conclusions are as follows:

1. A new non-contact polishing DC tool and CNNU slurry for small aperture curved surfaces were proposed, and the sub-nanometer roughness was achieved for the first time on NiP alloy aspheric optical mold by non-contact polishing method.

2. A simulation and material removal model of the DC tool non-contact polishing was established to clarify the relationship between MRR and working gap or tool speed during the polishing process. The calculation and experimental results show that the MRR decreases with the increment of the working gap and increases with the increasing tool speed. The maximum MRR reaches 0.016 μm/min at working gap 0.01 mm.

3. The formation mechanism of sub-nanometer roughness is clarified. The formation of sub-nanometer roughness is due to the semi-rigid damping cover of DC tool induced steady fluid and the synergistic effect of mechanical shearing and chemistry. The mechanical action is attributed to the micro-cutting of abrasive grains in the particle clusters and the chemical action is attributed to the continuous generation of nickel phosphate induced by hydrogen peroxide.

4. Surface roughness Sa 0.54 nm was achieved on the NiP alloy aspheric surface by using the proposed DC tool under the optimized parameters. Less than PV 600 nm form accuracy was achieved, which provides a new approach for current commercial applications. Higher form accuracy can be achieved by optimizing the DC toolpath and dwell time.

The future work will focus on two aspects: 1) The performance of the DC tool and CNNU slurry in polishing free-form optics will be investigated. 2) The subsurface damage suppression capability of DC tool and CNNU slurry will be further explored.

Funding. National Natural Science Foundation of China (51975096).

Disclosures. The authors declare no conflicts of interest.

Data availability. Data underlying the results presented in this paper are not publicly available at this time but may be obtained from the authors upon reasonable request.

References

1. W. Yang, Z. Zhang, W. Ming, L. Yin, and G. Zhang, "Study on shape deviation and crack of ultra-thin glass molding process for curved surface," Ceram. Int. **48**(5), 6767–6779 (2022).
2. D. W. Kim and J. H. Burge, "Rigid conformal polishing tool using non-linear visco-elastic effect," Opt. Express **18**(3), 2242–2257 (2010).
3. G. Ghosh, A. Sidpara, and P. Bandyopadhyay, "Review of several precision finishing processes for optics manufacturing," J. Micromanufac. **1**(2), 170–188 (2018).
4. J. Guo, S. Morita, M. Hara, Y. Yamagata, and T. Higuchi, "Ultra-precision finishing of micro-aspheric mold using a magnetostrictive vibrating polisher," CIRP Ann. **61**(1), 371–374 (2012).
5. Z. Wang, C. Shi, P. Zhang, Z. Yang, Y. Chen, and J. Guo, "Recent Progress of Advanced Optical Manufacturing Technology," Chin. J. Mech. Eng. **34**(1), 23–56 (2021).
6. Z. Xia, F. Fang, E. Ahearne, and M. Tao, "Advances in polishing of optical freeform surfaces: a review," J. Mater. Process. Technol. **286**, 116828 (2020).
7. J. Guo, H. J. H. Jong, R. Kang, and D. Guo, "Novel localized vibration-assisted magnetic abrasive polishing method using loose abrasives for V-groove and Fresnel optics finishing," Opt. Express **26**(9), 11608–11619 (2018).
8. L. Lunin, B. Sinel'nikov, and I. Sysoev, "Features of ion-beam polishing of the surface of sapphire," J. Synch. Investig. **12**(5), 898–901 (2018).
9. H. N. S. Yadav, M. Kumar, A. Kumar, and M. Das, "Plasma polishing processes applied on optical materials: A review," J. Micromanufac. 251659842110388 (2021).
10. Y. Xie and B. Bhushan, "Effects of particle size, polishing pad and contact pressure in free abrasive polishing," Wear **200**(1-2), 281–295 (1996).

Optics EXPRESS

11. J. Guo, X. Shi, C. Song, L. Niu, H. Cui, X. Guo, Z. Tong, N. Yu, Z. Jin, and R. Kang, "Theoretical and experimental investigation of chemical mechanical polishing of W–Ni–Fe alloy," Int. J. Extrem. Manuf. **3**(2), 025103 (2021).
12. H. Xiao, Y. Dai, J. Duan, Y. Tian, and J. Li, "Material removal and surface evolution of single crystal silicon during ion beam polishing," Appl. Surf. Sci. **544**, 148954 (2021).
13. M. Kumar, A. Kumar, A. Alok, and M. Das, "Magnetorheological method applied to optics polishing: A review," in *IOP Conference Series: Materials Science and Engineering* (IOP Publishing, 2020), p. 012012.
14. M. Li, B. Lyu, J. Yuan, C. Dong, and W. Dai, "Shear-thickening polishing method," Int. J. Mach. Tools Manuf. **94**, 88–99 (2015).
15. B. Lyu, Q. Shao, W. Hang, S. Chen, Q. He, and J. Yuan, "Shear thickening polishing of black lithium tantalite substrate," Int. J. Precis. Eng. Manuf. **21**(9), 1663–1675 (2020).
16. Selim Gürgen and Abdullah Sert, "Polishing operation of a steel bar in a shear thickening fluid medium," Composites, Part B **175**, 107127 (2019).
17. N. D. Nam, "Simulation Study on Polishing of Complex Surfaces by Non-Newtonian Fluids," in *2019 International Conference on System Science and Engineering (ICSSE)* (2019).
18. S. Yin, H. Jia, G. Zhang, F. Chen, and K. Zhu, "Review of small aspheric glass lens molding technologies," Front. Mech. Eng. **12**(1), 66–76 (2017).
19. W. L. Zhu and A. Beaucamp, "Non-Newtonian fluid based contactless sub-aperture polishing," CIRP Ann. **69**(1), 293–296 (2020).
20. W. L. Zhu and A. Beaucamp, "Generic three-dimensional model of freeform surface polishing with non-Newtonian fluids," Int. J. Mach. Tools Manuf. **172**, 103837 (2022).
21. F. Fang, N. Zhang, and X. Zhang, "Precision injection molding of freeform optics," Adv. Opt. Technol. **5**(4), 303–324 (2016).
22. M. Roeder, T. Guenther, and A. Zimmermann, "Review on fabrication technologies for optical mold inserts," Micromachines **10**(4), 233 (2019).
23. J. Chen, T. Sun, J. Su, J. Li, P. Zhou, Y. Peng, and Y. Zhu, "A novel agglomerated diamond abrasive with excellent micro-cutting and self-sharpening capabilities in fixed abrasive lapping processes," Wear **464-465**, 203531 (2021).
24. M. Li and J. Xie, "Green-chemical-jump-thickening polishing for silicon carbide," Ceram. Int. **48**(1), 1107–1124 (2022).
25. V. Sooraj and V. Radhakrishnan, "Investigations on the Application of Elastomagnetic Abrasive Balls for Fine Finishing," ASME J. Manuf. Sci. Eng. **137**(2), (2015).
26. G. Ghosh, A. Sidpara, and P. Bandyopadhyay, "High efficiency chemical assisted nanofinishing of HVOF sprayed WC-Co coating," Surf. Coat. Technol. **334**, 204–214 (2018).
27. H. Wei, C. Peng, H. Gao, X. Wang, and X. Wang, "On establishment and validation of a new predictive model for material removal in abrasive flow machining," Int. J. Mach. Tools Manuf. **138**, 66–79 (2019).
28. J. Wang, B. Lyu, L. Jiang, Q. Shao, C. Deng, Y. Zhou, J. Wang, and J. Yuan, "Chemistry enhanced shear thickening polishing of Ti–6Al–4 V," Precision Engineering **72**, 59–68 (2021).
29. Y. Ren, S. Yang, X. Huang, Y. Ming, and W. Li, "Research on the rheological characteristic of magnetorheological shear thickening fluid for polishing process," Int J Adv Manuf Technol **117**(1-2), 413–423 (2021).
30. M. Li, M. Liu, O. Riemer, B. Karpuschewski, and C. Tang, "Origin of material removal mechanism in shear thickening-chemical polishing," Int. J. Mach. Tools Manuf. **170**, 103800 (2021).
31. M. Li, F. Song, and Z. Huang, "Control strategy of machining efficiency and accuracy in weak-chemical-coordinated-thickening polishing (WCCTP) process on spherical curved 9Cr18 components," J. Manuf. Process. **74**, 266–282 (2022).
32. Z. Zhang, L. Liao, X. Wang, W. Xie, and D. Guo, "Development of a novel chemical mechanical polishing slurry and its polishing mechanisms on a nickel alloy," Appl. Surf. Sci. **506**, 144670 (2020).
33. K. H. Krishnan, S. John, K. Srinivasan, J. Praveen, M. Ganesan, and P. Kavimani, "An overall aspect of electroless Ni-P depositions - A review article," Metall and Mat Trans A **37**(6), 1917–1926 (2006).
34. F. Galindo-Rosales, F. Rubio-Hernández, and A. Sevilla, "An apparent viscosity function for shear thickening fluids," J. Non-Newtonian Fluid Mech. **166**(5-6), 321–325 (2011).
35. Q. Liu, R. Dong, H. Liu, F. Wang, D. Hu, and Y. Tian, "Optical element sub-surface defect detection combining fluorescence and scattering imaging," in *AOPC 2021: Optical Sensing and Imaging Technology* (SPIE, 2021), pp. 681–686.
36. D. D. Walker, D. Brooks, A. King, R. Freeman, R. Morton, G. McCavana, and S. W. Kim, "The 'Precessions' tooling for polishing and figuring flat, spherical and aspheric surfaces," Opt. Express **11**(8), 958–964 (2003).